Deciphering the complex paramagnetic NMR spectra of small laccase

Dasgupta, R.

Chapter 4

The resting oxidized state of small laccase analyzed with paramagnetic NMR spectroscopy

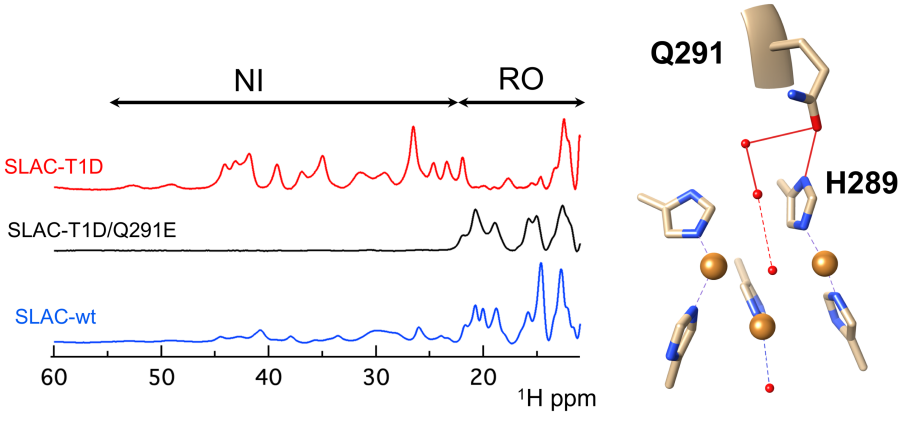

This chapter is published as:
Dasgupta, R., K.B.S.S. Gupta, H.J.M. de Groot, and M. Ubbink. 2021. The Resting Oxidized State of Small Laccase Analyzed with Paramagnetic NMR Spectroscopy. *ChemPhysChem*. 22:733–740. DOI: https://doi.org/10.1002/cphc.202100063

The enzyme laccase catalyzes the reduction of dioxygen to water at the trinuclear copper center (TNC). The TNC comprises a type-3 (T3) and a type-2 (T2) copper site. The paramagnetic NMR spectrum of the small laccase from *S. coelicolor* (SLAC) without the substrate shows a mixture of two catalytic states, the resting oxidized (RO) state and the native intermediate (NI) state. An analysis of the resonances of the RO state is reported. In this state, hydrogen resonances only of the T3 copper ligands can be found, in the region of 12 – 22 ppm. Signals from all six histidine ligands are found and can be attributed to Hδ1, Hβ or backbone amide H^N nuclei. Two sequence specific assignments are proposed on the basis of a second-coordination shell variant that also lacks the copper ion at the T1 site, SLAC-T1D/Q291E. This double mutant is found to be exclusively in the RO state, revealing a subtle balance between the RO and the NI states.

4.1 Introduction

The multicopper oxidase laccase can perform oxygen reduction with very little overpotential (~ 20 mV).(1) It comprises two active sites, a type-1 (T1) copper site to oxidize substrates and a tri-nuclear copper center (TNC) to reduce dioxygen to water. The TNC can be divided in a type-3 (T3) and a type-2 (T2) copper site. The T1 site is comprised of a single Cu(II) ion and is characterized by a strong 600 nm response in the absorption spectrum due to metal-sulfur transition between the Cu(II) and cysteine.(2) The T3 site has two interacting Cu(II) ions via a OH^- group while the T2 site has a single Cu(II) ion in a trigonal planar geometry coordinated to two histidine ligands and a water/OH^- group.(2) The current model of the reaction mechanism was previously described in detail (Figure 1.3).(3) In brief, the resting oxidized (RO) state is reduced to the fully reduced (FR) state by extracting four electrons from the substrates at the T1 site. The TNC has three cuprous ions in the FR state and can bind an oxygen molecule. Donation of two electrons from the TNC copper ions to the molecular oxygen leads to the formation of the peroxide intermediate (PI) state. At this stage the TNC needs one additional electron for complete oxygen reduction, which can be transferred from the reduced T1 site. In addition, for small laccase and human ceruloplasmin an electron can be transferred from the tyrosine residue near the T2 site, by forming a tyrosine radical.(4, 5) The two electron transfers coupled with a single proton transfer convert the PI state to the native intermediate (NI) state in which the peroxide bond between the oxygen atoms is broken. After three protons transfers from the protein environment, two water molecules are released and the NI state is converted into the RO state without the substrates, or into the FR state, with the substrates in the environment.

However, somewhat in contrast with this standard model, the NMR spectrum of a small laccase from *S. coelicolor* (SLAC) showed that the enzyme without substrate exists as a mixture of RO and NI states with all the copper ions in the cupric form (chapter 2 and 3).(6, 7) In the NI state, the T2 copper ion is coupled to the T3 copper ions via an oxygen atom (Figure 1.3 and S4.2b). The T2 copper ion is decoupled in the RO state (Figure 1.3. and S4.2a). The ^{1}H signals in the NMR spectrum of the RO state are less paramagnetically shifted (12 to 22 ppm) than those of the NI state (22 to 55 ppm).(6, 7) The wild type protein (SLAC-wt) is predominantly in the RO state, while the T1 site copper depleted mutant (SLAC-T1D the native, holoprotein, with copper ions in all sites) is mostly in the NI state (chapter 2 and 3).(6, 7) Five chemical exchange processes ascribed to ring motions of histidines coordinating coppers in both T3 and T2 sites were shown to be present for the NI state of SLAC-T1D (chapter 2 and 3).(7, 8) Further characterization of these exchange processes requires sequence specific assignment of the resonances to the histidine ligand nuclei. The assignment of the resonances is complicated by the paramagnetic nature of the copper ions, resulting in line broadening and hyperfine shifted resonances (up to 60 ppm in SLAC). This makes it impossible to use standard multidimensional NMR experiments for the assignments. Mutations in the second shell of coordination were considered as a means to obtain assignments. Using such a mutation, two of the chemical exchange processes in the NI state could be assigned to the T2 site histidines (chapter 3).(7) However, a detailed characterization of the RO state could not be done due to its low population in SLAC-T1D, resulting in the low S/N ratio of the corresponding resonances.(7)

In the current study, SLAC-wt is studied to characterize the RO state. The electronic coupling between the two coppers leads to fast electronic relaxation, yielding observable signals even for nuclei close to the metals.(9–11) The signals from nuclei in the T2 site ligands are broadened beyond detection because of the longer electronic relaxation time of the isolated electron spin on the copper.(7, 10, 12) The resonances from the T1 site are expected to be shifted to different spectral regions, 500 to 700 ppm for cysteine Hβ, 30 to 50 ppm for histidine ring, < 0 ppm for histidine Hβ and 12 to 20 ppm for other ligands(13–15). The signals from the T3 site are observed in the region from 12 to 22 ppm(6). They can be differentiated from the signals of the T1 site by their temperature dependence. T3 site signals have anti-Curie behavior, i.e. an increase in hyperfine coupling with increase in temperature, whereas the T1 site signals have Curie type behavior, i.e. a decrease in hyperfine coupling with increasing in temperature(12). The temperature dependence of the resonances in the 12-22 ppm region observed for the RO state was reported(6) and later shown to have anti-Curie. This suggests that all in that region arise from the T3 site ligands.

Using paramagnetically tailored NMR experiments and a mutation near the T3 site, the sequence specific assignment of two T3 site histidine ligands is reported for the RO state. In addition, resonances corresponding to all the six histidine ligands

of the T3 site could be found. Interestingly, the mutant enzyme is exclusively in the RO state, indicating that there is a subtle balance between the NI and RO states. Ultimately, assignment of the NMR resonances of nuclei at the heart of active site can lead to a better description of the TNC and aid in characterizing underlying motions, which may help to explain how laccases can so efficiently break the stable dioxygen bond.

4.2 Results and discussions

RO state in SLAC-wt

The NMR spectra of the RO state comprise signals from the T3 site histidine ligands that spans the spectral region between 12 and 22 ppm, while the NI state has signals from both the T3 and the T2 site histidine ligands in the spectral region between 22 and 55 ppm (chapter 3).(6, 7) The spectrum of SLAC-wt reveals a mixture of the NI and the RO states, similar to SLAC-T1D (chapter 3).(6, 7) The relative intensities of the signals in the RO and the NI spectral regions shows that SLAC-wt is predominantly in the RO state, contrary to SLAC-T1D. A Gaussian deconvolution of the ^{1}H spectral region between 10 and 22 ppm yields 14 resonances (Figure 4.1a). On the basis of 2D EXSY/NOESY (Figure 4.1b) and HMQC (Figure 4.1c) spectra, it can be concluded that some resonances derive from overlapping signals. The resonance at ~11 ppm is a superposition of proton signals (u0, c0, b0, e0 and x0), the resonances at ~16 ppm (u1 and b1) and 21.5 ppm (e2 and θ) are from two protons with strong overlap, and the resonance at ~19 ppm (b2, e1 and a2) is the summation of three proton signals. The cross-peaks between the resonances in the spectral region of 10 to 12 ppm have low S/N ratio and, therefore, we focus on the resonances in the region of 12 to 22 ppm for further analysis (a1, x1, d0, x2, u1, b1, c1, d1, b2, e1, a2, d2, c2, θ and e2) (Figure 4.1b). These resonances show anti-Curie behavior, where the hyperfine coupling increases with temperature (Figure 4.1e), which is well in line with previous observations.(6) Using the coupled two-metal center model (equation 1.2), the singlet-triplet energy gap was estimated to be $2J = -560$ cm^{-1} with $S = 0$ being the ground state and the $S = 1$ being the excited state. This is within the range of the reported values for the RO state of laccases (–550 to –620 cm^{-1}).(6, 7, 16) Extrapolation of the fitted curves to infinite temperature yields the diamagnetic chemical shifts (δ_{dia}).(12, 17, 18) On the basis of BMRB statistics, resonances related to the Hδ1, Hβ and backbone amide H^{N} protons of the T3 histidine ligand are distinguished (Figure 4.1e, see also Experimental Procedures in the Supporting Information). Resonances e2, c2, d2, b2, c1 and a2 derive from Hδ1, with a globally fitted δ_{dia} of 10 ppm, in line with the BMRB average for the histidine ring Hδ1 of 9.5 ppm. The resonances e1, d1, b1 and u1 are from Hβ with a δ_{dia} of 3.3 ppm matching the BMRB average of histidine Hβ of

3.2 ppm, while resonances a1, x2, d0 and x1 are attributed to backbone amide H^N with a δ_{dia} of 8.6 ppm with a BMRB average for the histidine backbone amide proton of 8.2 ppm. Assignments of resonances to nitrogen attached protons were validated by observation in a ^{15}N-^{1}H HMQC spectrum. Finally, an additional resonance θ is is poorly resolved due to strong overlap with resonance c2.

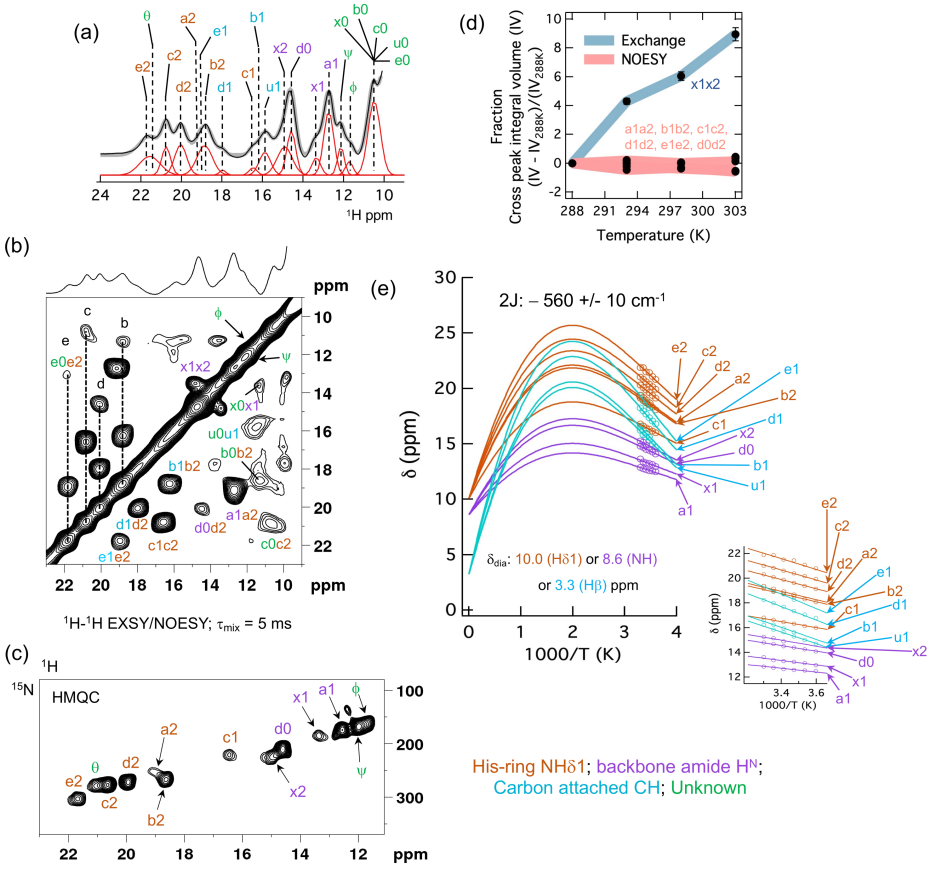

Figure 4.1*. NMR spectra of SLAC-wt. (a) 1D WEFT (19, 20) ^{1}H spectrum of the spectral region from 10 to 24 ppm corresponding to the RO state. The WEFT delay was set to 100 ms. Gaussian deconvolution is shown in red and the summation of the deconvoluted resonances is indicated with a solid grey trace; (b) 2D ^{1}H-^{1}H EXSY/NOESY spectrum at 298 K with mixing time (τ_{mix}) of 5 ms. The 1D ^{1}H spectrum is shown on top of the spectrum; (c) 2D ^{15}N-^{1}H HMQC spectrum. The delay for polarization transfer was set to 0.5 ms (7); (d) The temperature dependence of the fractional cross peak integrals to differentiate between the NOE and exchange cross peaks; (e) Temperature dependence of the chemical shift of the resonances marked in panels a, b and c. The solid lines represent the fit using equation S1. The 2J value and the diamagnetic chemical shifts are shown. The inset shows an enlargement of the experimental region. The corresponding hyperfine coupling constants A (MHz) are given in Table S4.3. The chemical shift values at different temperatures for each*

resonance in panel e is given in Table S4.4. The chemical shift values for resonances a2, x2, e1 and b1 were obtained from the temperature dependence of the cross peak in panel b. Color codes are given below panel d as brown for protons from the His-ring Hδ1, purple for the protons of the backbone amide H^N, cyan for the carbon attached protons and green for unknown. All spectra were recorded at 14 T.

The temperature dependence of the cross-peak intensities from the EXSY/NOESY spectrum shows that resonances x1 and x2 are in chemical exchange (Figure 4.1d), whereas other peaks are NOE cross peaks (a1a2, b1b2, c1c2, d0d2, d1d2 and e1e2). Cross peaks e1e2, d1d2 and b1b2 are the NOEs between the Hδ1 and Hβ protons, whereas cross peaks d0d2, and a1a2 are between the Hδ1 and backbone amide H^N protons. Cross peak c1c2 will be discussed further in the analyses of the double mutant SLAC-T1D/Q291E. Figure 4.1b shows that the resonances c, b, d and e have two cross peaks. The cross peaks e0e2, b0b2 and c0c2 could not be analyzed further due to their low S/N ratio but for resonance d NOE cross peaks are present between Hδ1 – Hβ and Hδ1 – backbone amide H^N protons (Figure 4.1b and e).

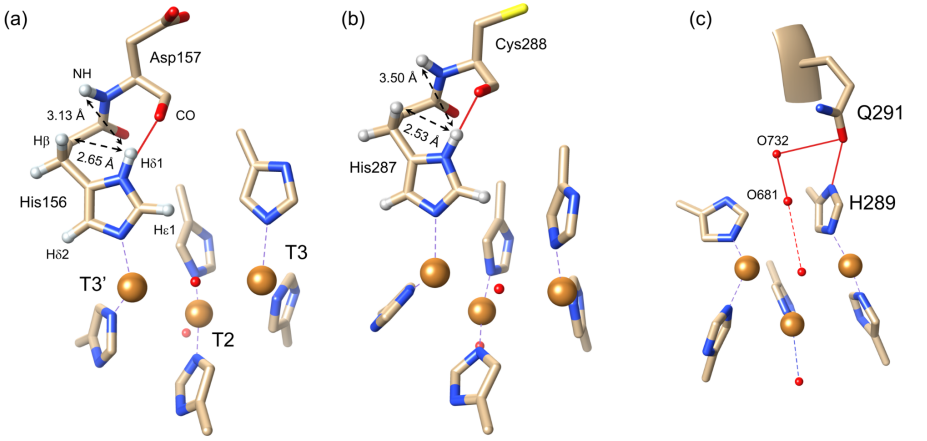

***Figure 4.2**. Histidine ligands in the TNC of SLAC. (a, b) Protons are shown near Hδ1 of His156 (a) and His287 (b) from the crystal structure of small laccase from S. coelicolor (PDB 3cg8)(15). Hydrogen bonds are shown as red lines. Amino acid residues are shown in golden sticks and copper ions as orange spheres. Distances between the Hδ1-Hβ and Hδ1-H^N are shown as double-sided arrows. Protons of the histidine ring are marked in panel a. The protons were modelled using the "AddH" algorithm as implemented in UCSF Chimera program(16) (for more details, see supporting information). His289 and 287 in panel a and His156 and 158 in panel b are not shown for clarity; (c) Hydrogen bonds are shown from Gln291 Oε1 to His289 Nδ1 and the bound water molecule O732 (red sphere), which is part of the water channel (Figure S4.3). O732 is hydrogen bonded to the next water molecule O681*

in the water channel. A possible hydrogen bond from O681 to the T3 site oxygen is shown as a red dashed line. His156, 158 and 102 are not shown for clarity.

Analysis of the crystal structure (PDB 3cg8) (21) of *S. coelicolor* SLAC reveals that in His156 and His287 (numbering from the crystal structure 3cg8) the Hδ1 proton is close to both Hβ and a backbone amide H^N proton (Figure 4.2), which could give rise to the observed NOE cross peak pairs for the d resonances. The Hδ1 proton of His156 is at 2.65 Å from the nearest Hβ proton and at 3.13 Å from the backbone amide H^N of Asp157. In His287, the Hδ1 proton is at 2.53 Å from the closest Hβ proton and at 3.50 Å from the backbone amide H^N of Cys288 (Figure 4.2). According to previous studies the resonances of nuclei in ligands of the T1 site, including Cys288, are subject to Curie behavior, and the hyperfine coupling decreases with increasing in temperature.(23) In contrast, resonance d0 shows an anti-Curie behavior (Figure 4.1e), which is generally observed for nuclei interacting with a coupled metal ion system.(12, 17, 18, 23) This suggests that the resonance d can be assigned to His156, showing NOEs between the Hδ1 - Hβ and Hδ1 - Asp157 H^N. The chemical shifts of the Hδ1, Hβ and Asp157 backbone amide H^N protons are 20, 18 and 14.5 ppm, with the paramagnetic shift contributions of about 10, 15 and 6 ppm, respectively. Interestingly, the paramagnetic contribution to the chemical shift of Hδ1 is less than for Hβ, although the former is four bonds away from the metal center, and the latter five. Perhaps this can be explained by (a) the higher electronegativity of nitrogen sequestering much spin density compared to carbon, resulting in less spin density on the nitrogen attached proton and (b) His156 Hδ1 having a strong hydrogen bond with the carbonyl CO of Asp157 that can result in an extended Nδ1-Hδ1 bond, thus further reducing the electron spin density on the proton. The shift of the H^N appears quite large for an FCS of a nucleus so many bonds away from the copper ion but it is noted that this is based on an estimate for the diamagnetic chemical shift of 8.6 ppm. Amide proton chemical shifts can vary widely. Also, a pseudo-contact shift could contribute to the observed shift.

Similar to the cross peak d0d2, a1a2 is also a NOE between a Hδ1 (a1, 12.68 ppm) and a backbone amide H^N proton (a2, 19.17 ppm). From the available crystal structures of small laccase, it is not possible to specifically assign it to any of the T3 histidine ligands. Cross peaks b1b2 and e1e2 can be from any of the remaining five T3 histidine ligands. Overall, resonances a, b, d (1-2) and e represent signals from four of the six T3 site histidine ligands, with resonance d (1-2) assigned to His156 and d0 to Asp 157 H^N (Table S4.1). A two-site, slow chemical exchange is observed for a backbone amide H^N proton (resonances x1 and x2, Figure 4.1). Although it is paramagnetically shifted, there are no NOE cross peaks with other resonances from the T3 site histidine ligands. In the state corresponding to x1, a weak cross peak is observed with resonance x0 (Figure 4.1b). It remains unclear to which nuclei these signals can be assigned.

Comparison between SLAC-wt and SLAC-T1D

Similar to SLAC-wt, the NMR spectrum of SLAC-T1D shows a mixture of the RO and the NI states.(6, 7) A strong response in the NI region (22 to 55 ppm) compared to the RO region (12 to 22 ppm) provides convincing evidence that SLAC-T1D is predominantly in the NI state (Figure 4.3a).(7) The proton resonances from the 1D ^{1}H WEFT spectra of the RO region in SLAC-T1D are not well resolved due to their low S/N ratio (Figure 4.3b). However, the RO spectral region in the 2D ^{1}H-^{1}H EXSY/NOESY spectra shows that the cross-peaks (a1a2, b1b2, c1c2, d1d2, e1e2 and x1x2) are present in both SLAC-T1D and SLAC-wt (Figure 4.3d). Cross-peak d0d2 is not observed in SLAC-T1D due to its low S/N ratio. The ^{15}N-^{1}H HMQC spectrum is also similar between the two proteins, although some changes can be observed (Figure 4.3e). In SLAC-T1D, resonances a1, x1, y, b2 and d2 are shifted downfield, while resonance x2 is shifted upfield in the proton dimension and resonance c1 is shifted downfield in the nitrogen dimension. Additional resonances w and z are observed in SLAC-T1D. A downfield shifted resonance is correlated to an increase in the spin density on the nucleus and vice-versa for an upfield shifted resonance.(12, 24) This suggests that in the RO state of SLAC-T1D, protons represented by resonances a1, x1, y, b2 and d2 have more spin density and x2 has less spin density compared to SLAC-wt. These changes can be attributed to the loss of the T1 copper in the T1D mutant, due to which the TNC is affected structurally and electronically.(6) Some structural change of the TNC is also suggested by the change in the singlet-triplet energy gap $2J = -560$ cm^{-1} for the RO state of SLAC-wt which is $2J = -600$ cm-1 for SLAC-T1D (7), because it was shown that a change in 2J value is related to the change in the angle between the hydroxyl bridged T3 copper ions (Cu^{2+}– OH^{-} – Cu^{2+}) and distance between the T3 coppers.(2, 3)

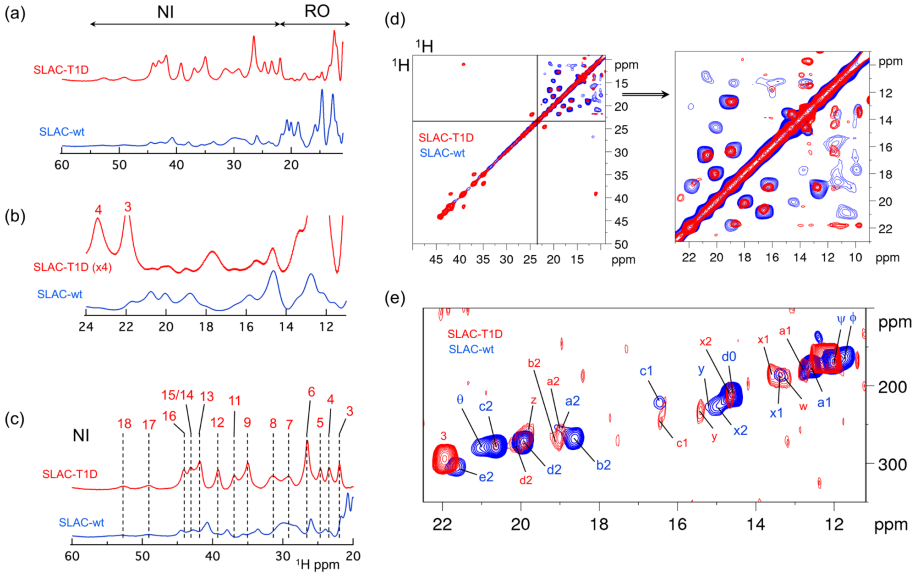

***Figure 4.3**: Comparison of SLAC-T1D and SLAC-wt. (a) Overlaid 1D ^{1}H spectra of SLAC-T1D (red) and SLAC-wt (blue). The spectral regions for the NI (22 to 55 ppm) and the RO (12 to 22 ppm) states are marked; (b) Expansion of the spectral region corresponding to the RO state where the spectral intensity of SLAC-T1D is multiplied by a factor 4; (c) Expansion of the spectral region corresponding to the NI state. The chemical shift values are given in Table S4.2 of the supporting information; (d) Overlaid ^{1}H-^{1}H EXSY/NOESY spectra of SLAC-wt and SLAC-T1D with an expansion of the spectral region 12 to 22 ppm. The resonance notations are in panel b of Figure 4.1; (e) Overlaid ^{15}N-^{1}H HMQC spectra for the RO region.*

The NI spectral region (22 to 55 ppm) of the 1D ^{1}H WEFT spectrum shows a similar pattern for SLAC-wt and SLAC-T1D. However, the resonances are broader for the SLAC-wt (Figure 4.3c). The resonances in SLAC-T1D are mostly downfield shifted compared to SLAC-wt, except for resonance 16, which is upfield shifted (Table S4.2). For resonances 17 and 18 the variation in chemical shifts are small compared to their large linewidth. In summary, resonances from RO and NI states can be observed for both SLAC-wt and SLAC-T1D proteins, consistent with the previous observations.(6, 7)

Analysis of SLAC-T1D/Q291E

It was shown that a mutation in the second coordination shell can help in assigning the complex paramagnetic NMR spectra of the nuclei in the TNC.(7) Using the SLAC-T1D/Y108F double mutant, the chemical exchange pairs 13-12 and 16-18 of the NI state (Figure 4.3c) were assigned to Hδ1 of His102 and His234 in the T2 site, respectively. (7) Following this method, a residue near the T3 site, Gln29, was mutated to aid in further assignment of the TNC ligands. A double mutant variant SLAC-T1D/Q291E was made to remove the effects of the T1 site copper. Gln291 is located near the T3 site of the TNC and its side chain is oriented toward the water channel leading into the TNC (Figure S4.3). This water channel has been proposed to be the source of protons in the formation of waters from dioxygen(21, 25). Gln291 also forms a strong hydrogen bond with the Nδ1 of His289 (Figure 4.2c), a ligand in the T3 site.

The 1D ^{1}H NMR spectrum of the double mutant SLAC-T1D/Q291E is compared with those of SLAC-T1D and SLAC-wt in Figure 4.4a. The NMR spectrum of the double mutant SLAC-T1D/Y108F was reported to be a mixture of the NI and the RO states with the NI state being the most populated, similar to the situation in SLAC-T1D(7). The NMR spectrum of SLAC-T1D/Q291E shows the enzyme to be exclusively in the RO state, without any signals from the NI state (Figure 4.4a).

A gaussian deconvolution of the ^{1}H spectral region between 12 and 24 ppm shows 11 resonances (Figure 4.4b). The 2D ^{1}H-^{1}H EXSY/NOESY spectrum (Figure 4.4d) reveals that the resonance ~14.5 ppm consists of two resonances, d0 and x2, and similarly, in resonance ~16.8 ppm c1' and b1 are overlaid. The response at ~19 ppm consists of four overlapping resonances d1, b2, e1 and a2. The temperature dependencies of the proton chemical shifts can be fitted to a coupled two-metal center model (equation 1.2) yielding a $2J = -560$ cm^{-1}, which is same for SLAC-wt (Figure 4.4e and 4.1e). The resonances could not be specifically assigned to His Hδ1, Hβ and backbone amide H^{N} protons from this temperature dependency due to substantial signal overlap (Figure 4.4b). However, the similarity between the spectra of SLAC-T1D/Q291E and SLAC-wt (Figure 4.5a) indicates comparable assignments.

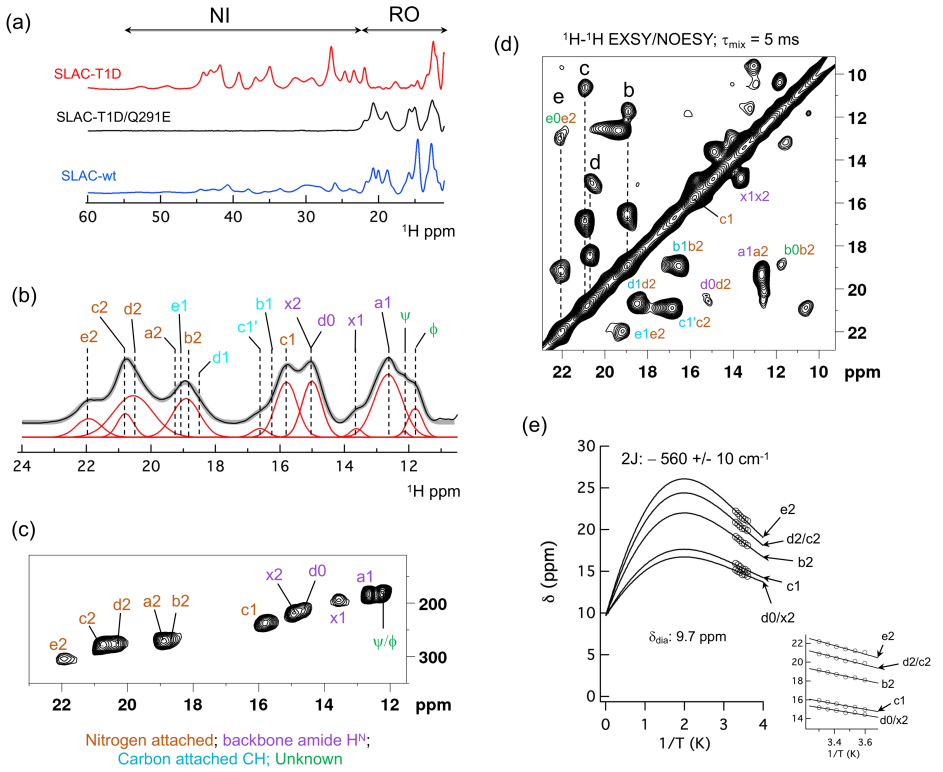

***Figure 4.4**: NMR spectra of SLAC-T1D/Q291E. (a) 1D ¹H spectra of SLAC-T1D (red), SLAC-T1D/Q291E (black) and SLAC-wt (blue). The spectral regions for the NI and the RO states are denoted; (b) 1D ¹H spectrum of SLAC-T1D/Q291E in the spectral region from 11 to 24 ppm. A Gaussian deconvolution is shown in red and the summation of the deconvoluted resonances is shown a solid grey trace; (c) ¹⁵N-¹H HMQC spectrum and (d) ¹H-¹H EXSY/NOESY spectrum of SLAC-T1D/Q291E for the ¹H spectral region of the RO state; (e) Temperature dependence of the resonances marked in panel b. The solid line is the fit to equation 1.5 (for more details see the Experimental procedures in the supporting information). The inset shows an enlargement of the data region. The 2J value and the diamagnetic chemical shifts are shown. The corresponding hyperfine coupling constants A (MHz) are given in Table S4.3. The chemical shifts at different temperatures for each resonance in panel e are given in Table S4.5. The color code and the assignments are same as in Figure 4.1.*

Overlaid NMR spectra of SLAC-wt and SLAC-T1D/Q291E reveal the changes in the RO state of the protein due to the Q291E mutation. The ¹H resonances for SLAC-T1D/Q291E are broader than for SLAC-wt (Figure 4.5a). Chemical shift perturbations are clear from the 2D ¹H-¹H EXSY/NOESY spectra, showing that resonances b2, c2, d0, d2, e2, x1 and x2 are downfield shifted, while resonance c1 is upfield shifted and resonance a1 is unperturbed (Figure panels 4.5b and 4.5d). Most of the resonances are

downfield shifted, suggesting that the Q291E mutation leads to an increase in the spin density delocalization over the ligands in the TNC. It is of interest to note the ^{1}H-^{1}H cross peak c1c2 in SLAC-wt and c1'c2 in SLAC-T1D/Q291E. In the 2D ^{15}N-^{1}H HMQC, the resonance assigned as c1 in SLAC-wt is upfield shifted in the proton dimension and downfield shifted in the nitrogen dimension in the equivalent spectrum of SLAC-T1D/Q291E (Figure 4.5c). However, in the EXSY/NOESY spectrum the cross peak for c1c2 moves slightly downfield in the c1 dimension (Figure 4.5b). This cross-peak was assigned as c1'c2 in SLAC-T1D/Q291E and since c1' is suppressed in the HMQC data compared to the EXSY/NOESY spectrum it can be attributed to a carbon attached proton (Figure 4.4c). It is therefore concluded that the resonances c1 and c1' are overlapped in SLAC-wt (Figure 4.1b and 4.5b), whereas in the spectrum of SLAC-T1D/Q291E they can be distinguished (Figure 4.5c). Resonances c1 and c1' may well belong to different histidines. The temperature dependence of the chemical shift showed that resonance c1 derives from a Hδ1 nucleus. The resonance c2 also derives from a Hδ1 nucleus and because c1' can be attributed to a carbon attached hydrogen, the c1'c2 cross-peak is likely to represent another Hδ1-Hβ NOE from one of the T3 His ligands.

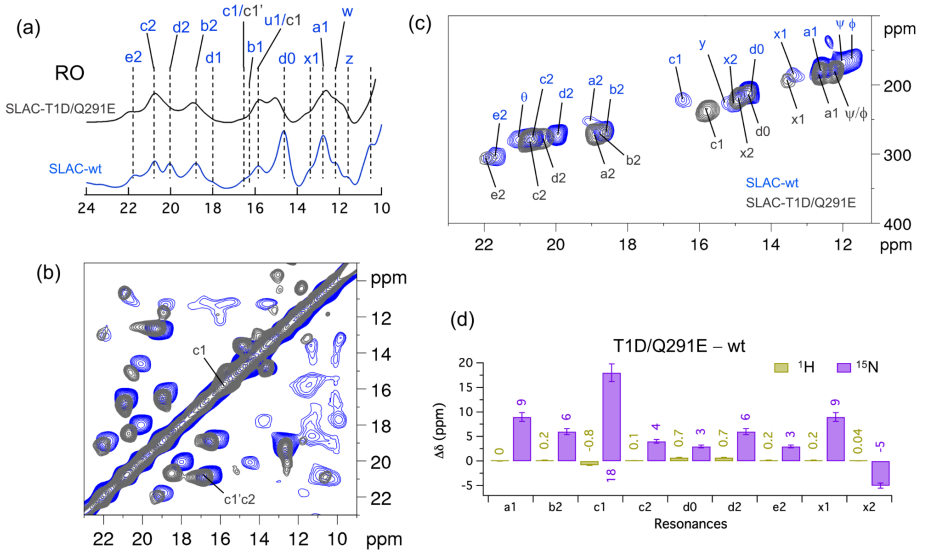

***Figure 4.5**: Comparison of SLAC-T1D/Q291E and SLAC-wt. Overlaid 1D ^{1}H NMR spectra (a), 2D ^{1}H-^{1}H EXSY/NOESY with the resonances c1, c1' and c2 marked (b) and ^{15}N-^{1}H HMQC with all the resonances marked (c) of SLAC-T1D/Q291E (black) and SLAC-wt (blue) of the spectral region 10 to 23 ppm; (d) Chemical shift perturbations as the difference in chemical shift between SLAC-T1D/Q291E and SLAC-wt.*

The chemical shift perturbations between SLAC-T1D/Q291E and SLAC-wt show that the strongest perturbation is for the resonance c1. Since Gln291 has a strong hydrogen bond with His289 (Figure 4.2c), the Q291E mutation can have a pronounced effect on the chemical shift of its Nδ1 and Hδ1 nuclei. Due to the negative charge, Glu291 is likely to have a stronger hydrogen bond with the Hδ1 of His289, increasing the N-H bond length and reducing the spin density on the proton while increasing it on the nitrogen. This will result in an upfield shift for the proton and a downfield shift for nitrogen, in line with the observation in the HMQC spectrum (Figure 4.5c). Therefore, we propose that resonance c1 is from Hδ1 of His289 in the T3 site.

4.3 Conclusion

The NMR spectrum of SLAC-wt is a mixture of the RO and the NI states, and the intensity profile shows that the RO state is most populated. Paramagnetically tailored NMR experiments and the double mutant SLAC-T1D/Q291E helped to provide residue specific assignments for the Hδ1 nuclei of all the six histidine ligands of the T3 site (a2, b2, c1, c2, d2 and e2). The resonances d1 and d2 are assigned to His156 Hβ and Hδ1, respectively, d0 to Asp 157 H^N and resonance c1 is assigned to His289 Hδ1. Cross peaks in the ^1H spectral region of 10-12 ppm could not be analyzed due to their low S/N ratio. Some of the cross peaks (b0b2, c0c2 and u0u1) are associated with resonances assigned to the T3 histidine ligands. Assuming that b0, c0 and u0 arise from the backbone amide H^N protons, cross peaks b0b2 and c0c2 might be NOEs between the His Hδ1 (b2 and c2) and backbone amide protons (b0 and c0). Cross peak u0u1 may be a NOE between a Hβ and a H^N.

Chapter 2 and 3 shows the presence of five chemical exchange processes in the NI state involving Hδ1 protons and attributed to His ring motions.(7, 8) In the RO state, these exchange processes are not observed. Perhaps the exchange is still present but not visible because the lower spin density on nuclei causes smaller FCS. For the NI state, the differences in chemical shift between the states represent ~10% of the FCS. The differences in chemical shift between the different states may be too small in the RO state to result in observable exchange peaks. Alternatively, the RO state may be more rigid, slowing down His ring motions sufficiently to bring the exchange rate outside the window that results in exchange cross peaks (80 – 200 s^{-1}). For the RO state, one exchange process was observed, between signals x1 and x2. However, these resonances do not derive from Hδ1 but from a shifted backbone amide signal. It provides evidence that some motion is occurring in the RO state as well, but we have not been able to assign it to a particular nucleus. We expect that the use of second coordination shell mutations can allow further assignment of the paramagnetic NMR signals from the TNC, providing spectroscopic probes that can help to

understand how motions of the histidine ligands assist in progressing rapidly through the consecutive steps of the catalytic cycle.

4.4 Supporting Information

Site directed mutagenesis

The plasmid pET-20b containing the gene encoding SLAC-T1D (pET-20b/SLAC-T1D) (8) was used as a template to prepare the double mutant SLAC-T1D/Q291E. A two-fragment Gibson assembly (26) approach was used for the site directed mutagenesis. The primers used for the mutagenesis are as follows:

Q291E (mutation is given in bold):
Forward primer: 5'– G TAC CAC AGC CAC GTC **GAA** AGC CAC TCC GAC ATG – 3'
Reverse primer: 5'– CAT GTC GGA GTG GCT **TTC** GAC GTG GCT GTG GTA C – 3'
Primers for generating two-fragments:
pTarget-split-Forward primer: 5'– AAATACTGTCCTTCTAGTGTAGCCGTAGTTAG – 3'
pTarget-split-Reverse primer: 5'– TTCTTGAAGTGGTGGCCTAACTACGG – 3'

Two parts of the pET-20b/SLAC-T1D plasmid were PCR-amplified. Fragment 1 was amplified using the Q291E-forward and pTarget-split-Reverse primers and fragment 2 using the Q291E-reverse and pTarget-split-Forward primers. The resulting fragments (2585 and 2548 base pairs, respectively) were extracted from an agarose gel using GFX™ PCR DNA and Gel Band Purification Kit (Merck, Germany) and combined using Gibson assembly master mix at 50°C.(26) The resulting plasmid pET-20b/SLAC-T1D/Q291E was introduced in the DH5α strain of *Escherichia coli* for propagation. The desired mutation was confirmed by DNA sequencing (BaseClear, Leiden, The Netherlands).

Protein expression and purification

^{15}N uniformly labelled SLAC-wt, SLAC-T1D and SLAC-T1D/Q291E were produced and purified as described previously.(7, 8) Purity was checked using SDS PA-gel electrophoresis and a band ~ 74 kDa was observed in each case (Figure S4.1). This corresponds to the molecular weight of a dimer. However, under native conditions, the molecular weight of the proteins was ~ 105 kD as determined by size-exclusion chromatography coupled to multi-angle light scattering detection, in line with the expected trimeric form.(21)

NMR spectroscopy

Samples contained ~1 mM of protein in 10 mM sodium phosphate buffer pH 7.3 with 10% D_2O. 1D ^1H water eliminated Fourier transform, 2D ^1H-^1H EXSY/NOESY and 2D ^1H-^{15}N HMQC spectra were obtained as described previously.(7, 8) Experiments were carried on a Bruker AV-III HD 600 MHz NMR spectrometer equipped with a TXI cryoprobe.

Modelling protons

The protons were modelled in the crystal structure 3cg8 using "AddH" algorithm as implemented in UCSF Chimera program.(22) The hydrogen bonds were taken into consideration and the protonation states of histidine were kept unspecified so that the program can add hydrogens based on the hydrogen bonds and steric clash.

Temperature dependence of the chemical shift

For two cupric coppers at close distance, antiferromagnetic coupling results in a $S = 0$ state at low temperature. At ambient temperature, the $S = 1$ state can be populated. The energy gap between the two states is given by the coupling constant $2J$ (in cm^{-1}). The observed chemical shift, δ_{obs}, depends on the spin density on the nucleus, given by A, the isotropic hyperfine coupling constant, and value of $2J$ according to equation 1.2. For the temperature dependency of the resonances from SLAC-wt in Figure 4.1e of the main text a global fit algorithm as implemented in IGOR pro 6.37 was used to fit the data by linking the $2J$ values for all the resonances. This resulted in an estimation of δ_{dia} for respective resonances at $k_BT >>> 2J$. These were grouped as His ring Hδ1, His Hβ and H^N by comparison to the chemical shifts obtained from the BMRB statistics, where δ_{dia} for Hδ1, Hβ and H^N are 9.5, 3.2 and 8.2 ppm, respectively. For the final global fit, the $2J$ values for all the data were linked and the δ_{dia} values were linked for resonances belonging to the same type, being Hδ1, Hβ or H^N. For the resonance from SLAC-T1D/Q291E, the $2J$ values and the δ_{dia} were linked for all. The only variable that was not linked during the global fit was A in both the proteins.

Supporting figures and tables

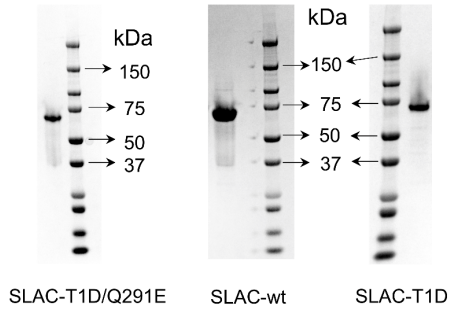

***Figure S4.1**: Image of Bis-Tris precast SDS PAGE-gels (ThermoFischer Scientific) of purified SLAC-T1D/Q291E, SLAC-wt and SLAC-T1D.*

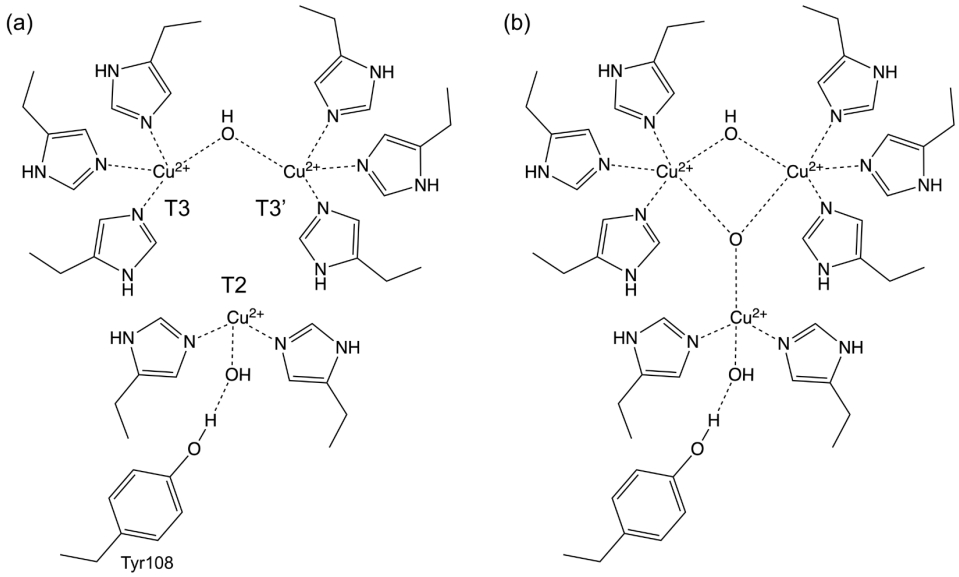

***Figure S4.2**: Schematic of the TNC in (a) the resting oxidized (RO) state and (b) the native intermediate (NI) state. The Tyr108 residue and respective coppers are marked in panel a. The numbering is adopted from the crystal structure 3cg8 (from S. coelicolor, resolution 2.68 Å).(21)*

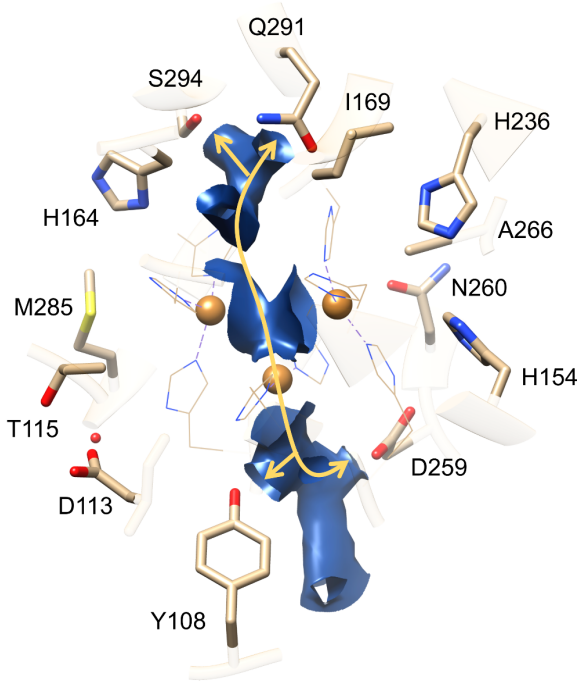

***Figure S4.3**: The second shell residues at the TNC in SLAC from S. coelicolor (PDB 3cg8). (21) The water channel is shown as the electron density surface of the water molecules in the TNC. (25) The double-sided arrows show possible proton transfer paths. Coordinating histidine ligands are shown as wire and the second coordination sphere residues are shown as sticks. The red sphere is a water molecule. The copper ions are shown as orange spheres.*

***Table S4.1**: Chemical shift (ppm) of the resonances in the ^{1}H spectral region of 12 to 22 ppm attributed to the T3 site histidine ligands from SLAC-wt and SLAC-T1D/Q291E at 298 K. The type of protons associated with the resonances are indicated. Hδ1 and Hβ are from histidine and H^{N} is a backbone amide proton. Assignment of resonance c1 and d (d0, d1 and d2) to specific histidine is also indicated. The numbering is adopted from the crystal structure of SLAC from S. coelicolor PDB 3cg8.(21)*

		SLAC-wt		SLAC-T1D/Q291E		Proton	Assignment
	Resonance	^{1}H	^{15}N	^{1}H	^{15}N		Numbering from PDB 3cg8
T3 site histidine ligands	a1	12.68	175	12.68	185	H^{N}	
	a2	19.17	256	19.37	274	Hδ1	
	b1	16.25	-	16.52	-	Hβ	
	b2	18.80	268	18.96	274	Hδ1	
	c1	16.56	221	15.80	240	Hδ1	His289
	c1'	ol	-	16.84	-	Hβ	
	c2	20.81	278	20.95	283	Hδ1	
	d0	14.48	212	15.14	215	H^{N}	Asp 157
	d1	17.99	-	18.47	-	Hβ	His 156
	d2	20.07	272	20.07	280	Hδ1	
	e1	18.96	-	19.16	-	Hβ	
	e2	21.8	304	22.02	307	Hδ1	
	x1	13.43	187	13.66	197	H^{N}	
	x2	14.83	225	14.95	221	H^{N}	

ol: overlap with c1

***Table S4.2**: Chemical shift in ppm for the resonances in the ^1H spectra region of 22 to 55 ppm belonging to the NI state of SLAC-T1D and SLAC-wt at 298 K.*

Resonance	SLAC-T1D	SLAC-wt
3	21.94	Overlap with resonance e2
4	23.42	23.33
5	24.70	23.91
6	26.52	25.96
7	29.27	28.52
8	31.48	30.14
9	34.99	33.67
11	36.95	35.66
12	39.21	37.96
13	41.86	40.72
14/15	43.14	42.83
16	44.07	44.43
17	49.21	49.21
18	52.77	52.77

***Table S4.3**: Hyperfine coupling constants (A) obtained from fitting the temperature dependencies of the chemical shifts to equation 1.5 for SLAC-wt and SLAC-T1D/Q291E. The error values are ~ 5% from the fit.*

SLAC-wt		SLAC-T1D/Q291E	
Resonance	*A* (MHz)	Resonance	*A* (MHz)
a1	0.7	d0/x2	0.9
x1	0.8	c1	1.0
u1	2.1	b2	1.6
b1	2.2	d2/c2	1.9
d0	1.0	e2	2.0
x2	1.1		
d1	2.5		
c1	1.1		
a2	1.5		
e1	2.6		
b2	1.5		
d2	1.7		
c2	1.8		
e2	2.0		

***Table S4.4**: Chemical shift at different temperatures for the resonances in the RO state of SLAC-wt.*

	Temperature (K)					
	278	283	288	293	298	303
Resonance	Chemical shift (ppm)					
e2	20.81	21.08	21.44	21.51	21.88	21.89
c2	19.93	20.17	20.40	20.62	20.84	21.01
d2	19.13	19.38	19.63	19.87	20.09	20.32
b2	18.06	18.30	18.52	18.75	18.91	19.14
d1	16.80	17.06	17.35	17.70	17.99	18.24
c1	16.00	16.14	16.32	16.46	16.64	16.81
u1	14.70	15.00	15.30	15.63	15.83	16.23
x2	ol	ol	ol	14.90	15.15	15.26
d0	14.08	14.25	14.40	14.51	14.67	14.81
x1	12.97	13.14	13.23	13.29	13.38	13.63
a1	12.50	12.55	12.58	12.65	12.76	12.86
b1	ol	ol	15.63	15.95	16.25	16.60
a2	ol	ol	18.65	18.90	19.13	19.34
e1	ol	ol	18.27	18.70	18.94	19.37

ol: Chemical shift could not be determined due to resonance overlap

***Table S4.5**: Chemical shift at different temperatures for the resonances in the RO state of SLAC-T1D/Q291E.*

	Temperature (K)					
	278	283	288	293	298	303
Resonance	Chemical shift (ppm)					
e2	21.057	21.219	21.408	21.662	21.927	22.213
d2/c2	19.897	20.115	20.153	20.438	20.673	20.884
b2	18.112	18.347	18.423	18.717	18.928	19.172
c1	14.984	15.234	15.275	15.578	15.758	15.952
d0/x2	14.438	14.651	14.628	14.882	15.015	15.183

4.5 References

1. Mano, N., V. Soukharev, and A. Heller. 2006. A Laccase-Wiring Redox Hydrogel for Efficient Catalysis of O $_2$ Electroreduction. *J. Phys. Chem. B*. 110:11180–11187.
2. Solomon, E.I., D.E. Heppner, E.M. Johnston, J.W. Ginsbach, J. Cirera, M. Qayyum, M.T. Kieber-Emmons, C.H. Kjaergaard, R.G. Hadt, and L. Tian. 2014. Copper Active Sites in Biology. *Chemical Reviews*. 114:3659–3853.
3. Solomon, E.I., A.J. Augustine, and J. Yoon. 2008. O2 Reduction to H2O by the multicopper oxidases. *Dalton Trans*. 3921–3932.
4. Gupta, A., I. Nederlof, S. Sottini, A.W.J.W. Tepper, E.J.J. Groenen, E.A.J. Thomassen, and G.W. Canters. 2012. Involvement of Tyr108 in the Enzyme Mechanism of the Small Laccase from Streptomyces coelicolor. *Journal of the American Chemical Society*. 134:18213–18216.
5. Tian, S., S.M. Jones, and E.I. Solomon. 2020. Role of a Tyrosine Radical in Human Ceruloplasmin Catalysis. *ACS Cent. Sci.*
6. Machczynski, M.C., and J.T. Babicz. 2016. Correlating the structures and activities of the resting oxidized and native intermediate states of a small laccase by paramagnetic NMR. *Journal of Inorganic Biochemistry*. 159:62–69.
7. Dasgupta, R., K.B.S.S. Gupta, H.J.M. de Groot, and M. Ubbink. 2020. Towards resolving the complex paramagnetic NMR spectrum of small laccase: Assignments of resonances to residue specific nuclei. *Magnetic Resonance Discussions*. 1–13.
8. Dasgupta, R., K.B.S.S. Gupta, F. Nami, H.J.M. de Groot, G.W. Canters, E.J.J. Groenen, and M. Ubbink. 2020. Chemical Exchange at the Trinuclear Copper Center of Small Laccase from Streptomyces coelicolor. *Biophysical Journal*. 119:9–14.
9. Bubacco, L., J. Salgado, A.W.J.W. Tepper, E. Vijgenboom, and G.W. Canters. 1999. ^{1}H NMR spectroscopy of the binuclear Cu(II) active site of Streptomyces antibioticus tyrosinase. *FEBS Letters*. 442:215–220.
10. Murthy, N.N., K.D. Karlin, I. Bertini, and C. Luchinat. 1997. NMR and Electronic Relaxation in Paramagnetic Dicopper(II) Compounds. *J. Am. Chem. Soc.* 119:2156–2162.
11. Maekawa, M., S. Kitagawa, M. Munakata, and H. Masuda. 1989. Nuclear magnetic resonance studies of dicopper(II) complexes with binucleating ligands containing imidazoles. *Inorg. Chem*. 28:1904–1909.
12. Bertini, I., C. Luchinat, G. Parigi, and E. Ravera. 2017. NMR of paramagnetic molecules: applications to metallobiomolecules and models. Second edition. Amsterdam: Elsevier.
13. Kalverda, A.P., J. Salgado, C. Dennison, and G.W. Canters. 1996. Analysis of the paramagnetic copper(II) site of amicyanin by 1H NMR spectroscopy. *Biochemistry*. 35:3085–3092.
14. Canters, G.W., H.A.O. Hill, N.A. Kitchen, and E.T. Adman. 1984. The assignment of the 1H nuclear magnetic resonance spectrum of azurin. An investigation of the 1H NMR spectrum of the blue copper protein, azurin, from Pseudomonas aeruginosa, with reference to the previously determined crystal structure. *European Journal of Biochemistry*. 138:141–152.
15. Bertini, I., S. Ciurli, A. Dikiy, R. Gasanov, C. Luchinat, G. Martini, and N. Safarov. 1999. High-Field NMR Studies of Oxidized Blue Copper Proteins: The Case of Spinach Plastocyanin. *Journal of the American Chemical Society*. 121:2037–2046.
16. Quintanar, L., J. Yoon, C.P. Aznar, A.E. Palmer, K.K. Andersson, R.D. Britt, and E.I. Solomon. 2005. Spectroscopic and Electronic Structure Studies of the Trinuclear Cu Cluster Active Site of the Multicopper Oxidase Laccase: Nature of Its Coordination Unsaturation. *J. Am. Chem. Soc.* 127:13832–13845.
17. Bertini, I., C. Luchinat, L. Messori, and M. Vasak. 1989. Proton NMR spectra of the Co4S11 cluster in metallothioneins: a theoretical model. *J. Am. Chem. Soc.* 111:7300–7303.
18. Banci, L., I. Bertini, and C. Luchinat. 1990. The 1H NMR parameters of magnetically coupled dimers—The Fe2S2 proteins as an example. In: Bioinorganic Chemistry. Berlin, Heidelberg: Springer. pp. 113–136.
19. Patt, S.L., and B.D. Sykes. 1972. Water Eliminated Fourier Transform NMR Spectroscopy. *J. Chem. Phys.* 56:3182–3184.
20. Bertini, I., C. Luchinat, G. Parigi, and R. Pierattelli. 2005. NMR Spectroscopy of Paramagnetic Metalloproteins. *ChemBioChem*. 6:1536–1549.

21. Skálová, T., J. Dohnálek, L.H. Østergaard, P.R. Østergaard, P. Kolenko, J. Dušková, A. Štěpánková, and J. Hašek. 2009. The Structure of the Small Laccase from Streptomyces coelicolor Reveals a Link between Laccases and Nitrite Reductases. *Journal of Molecular Biology*. 385:1165–1178.
22. Pettersen, E.F., T.D. Goddard, C.C. Huang, G.S. Couch, D.M. Greenblatt, E.C. Meng, and T.E. Ferrin. 2004. UCSF Chimera—A visualization system for exploratory research and analysis. *Journal of Computational Chemistry*. 25:1605–1612.
23. Banci, L., I. Bertini, C. Luchinat, R. Pierattelli, N.V. Shokhirev, and F.A. Walker. 1998. Analysis of the Temperature Dependence of the 1H and 13C Isotropic Shifts of Horse Heart Ferricytochrome c: Explanation of Curie and Anti-Curie Temperature Dependence and Nonlinear Pseudocontact Shifts in a Common Two-Level Framework. *J. Am. Chem. Soc.* 120:8472–8479.
24. Bertini, I., C. Luchinat, and G. Parigi. 2002. Magnetic susceptibility in paramagnetic NMR. *Progress in Nuclear Magnetic Resonance Spectroscopy*. 40:249–273.
25. Gabdulkhakov, A., I. Kolyadenko, O. Kostareva, A. Mikhaylina, P. Oliveira, P. Tamagnini, A. Lisov, and S. Tishchenko. 2019. Investigations of Accessibility of T2/T3 Copper Center of Two-Domain Laccase from Streptomyces griseoflavus Ac-993. *International Journal of Molecular Sciences*. 20:3184.
26. Gibson, D.G., L. Young, R.-Y. Chuang, J.C. Venter, C.A. Hutchison, and H.O. Smith. 2009. Enzymatic assembly of DNA molecules up to several hundred kilobases. *Nature Methods*. 6:343–345.